P2.4 INVESTIGATION OF A VISIBLE REFLECTANCE PARAMETERIZATION FOR DETERMINING CLOUD PROPERTIES IN MULTI-LAYERED CLOUDS

Robert F. Arduini
SAIC, Hampton, VA 23666

Patrick Minnis, David F. Young
NASA Langley Research Center, Hampton, VA 23681

1. INTRODUCTION

The techniques employed to routinely derive cloud properties from satellite data for ARM and the Clouds and the Earth's Radiant Energy System (CERES) use parameterizations of cloud reflectance and effective emittance determining the optical depth and effective particle size of clouds. These retrievals typically assume that the cloud in a given pixel is a single-layered plane-parallel cloud. Because overlapped clouds are common, this assumption often results in cloud properties that represent some mixture of the multi-layered cloud properties and do not provide an accurate assessment of actual cloud properties in the scene. Various methods using combinations of infrared and solar channels (Baum et al. 2000) and solar and microwave data (Lin et al. 1999) have been developed to detect multi-layered clouds. Once identified, it is necessary to unscramble the properties for each of the cloud layers. If it is assumed that the properties of the lower layer cloud are known, it should be possible to derive the properties of the upper-level cloud from either infrared or visible data. This paper investigates the potential for deriving the upper-cloud optical depth using the latest visible reflectance parameterization used for the CERES and ARM analyses.

2. VISIBLE REFLECTANCE PARAMETERIZATION

A new parameterization was developed to improve the accuracy of the estimated top-of-atmosphere (TOA) reflectances for clouds over dark and bright surfaces compared to those from a detailed adding-doubling (AD) radiative transfer model (RTM; see Minnis et al. 1993). This parameterization is based on the AD equations using the same lookup tables developed as in Minnis et al. (1998) that include the diffuse cloud albedo $\alpha_{cd}(\tau, r)$, cloud albedo $\alpha_c(\tau, r, \theta_o)$, and the cloud reflectance $\rho(\tau, r, \theta_o, \theta, \phi)$, where τ and r are the cloud visible optical depth and effective particle size , respectively. The solar and viewing zenith and relative azimuth angles are θ_o, θ, and ϕ, respectively. The parameterization also uses the lookup tables of atmospheric reflectance $\rho_R(\tau_R, \theta_o, \theta, \phi)$, albedo $\alpha_R(\tau_R, \theta_o)$, and diffuse albedo $\alpha_{Rd}(\tau_{DR}, \theta_o)$ due to Rayleigh scattering (Minnis et al. 1993). The parameterization assumes the atmosphere is divided into three layers with a lower surface. The top layer, designated layer 1, and layer 3 are Rayleigh scattering layers, while layer 2 is the cloud layer.

The reflectance for two adjacent layers is computed using the adding equations. The combined reflectance for the top Rayleigh layer and the cloud layer is

$$R_{12} = \rho_{R1} + \alpha_c' D_1(1 - \alpha_{Rd1}) + t_{R1}(\mu)\,[t_{R1}(\mu_o)\,\rho_c + S_1] \quad (1)$$

where

$\alpha_c' = \alpha_c\, t_{R1}(\mu_o) + [1 - t_{R1}(\mu_o)]\,\alpha_{cd}$,
$D_1 = T_1\,(1 + S_1)$,
$S_1 = \alpha_{Rd1}\,\alpha_{cd} / (1 - \alpha_{Rd1}\,\alpha_{cd})$,
$T_1 = 1 - t_{R1}(\mu_o) - \alpha_{R1}$,
$\mu, \mu_o = \cos\theta, \cos\theta_o$,

t_R is the direct Rayleigh transmission as defined by Minnis et al. (1993), and the numeric indices refer to a layer or combination of layers. The downward transmittance of the two layers is

$$T_{12} = D_1\,[T_2 + t_c(\mu)] + T_2\,t_{R1}(\mu_o),$$

where

$T_2 = 1 - \alpha_c' - t_c(\mu_o)$

and t_c is the direct transmittance of the cloud (Minnis et al. 1993).

The combined reflectance for the three layers is

$$R_{123} = R_{12} + \alpha_{Rd2}\,D_2\,T_{12}^* + (\rho_{R2}\,t_c(\mu_o)\,t_{R1}(\mu_o) + S_2)\,t_c(\mu)\,t_{R1}(\mu),$$

where

$D_2 = T_{12}\,(1 + S_2)$,
$S_2 = Q_2 / (1 - Q_2)$,
$Q_2 = \alpha_{Rd2}\,R_{12}'$,
$R_{12}' = \alpha_{R1} + (1 - \alpha_{Rd1})D_1\,\alpha_{cd} + t_{R1}(\mu)[\alpha_{cd}\,t_{R1}(\mu_o) + S_1)$
$T_{12}^* = U_1^*\,(1 - \alpha_{Rd1})$,

and

$U_1^* = (1 - \alpha_{cd})\,(1 + S_1)$.

The downward transmittance for the three layers is

$$T_{123} = D_2\,[T_3 + t_c(\mu)] + T_2\,t_{R1}(\mu_o),$$

where

$$T_3 = 1 - \alpha_{Rd2} - t_{R2}(\mu_o).$$

*Corresponding author address: Robert F. Arduini, SAIC, 1 Executive Parkway, Hampton, VA 23666. email: r.f.arduini@larc.nasa.gov.

The combined atmosphere and surface reflectance is

$$R_{as} = R_{123} + \alpha_{sd} T_{123}^{*} D_3 + t_{123}(\mu)[\rho_s\, t_{123}(\mu_o) + S_3], \quad (2)$$

where α_{sd} and ρ_s are the diffuse surface albedo and surface bidirectional reflectance, respectively,

$t_{123}(\mu) = t_{R1}(\mu)\, t_c(\mu)\, t_{R3}(\mu)$
$t_{123}(\mu_o) = t_{R1}(\mu_o)\, t_c(\mu_o)\, t_{R3}(\mu_o)$
$D_3 = T_{123}\,(1 + S_3)$,
$S_3 = Q_3 / (1 - Q_3)$
$Q_3 = \alpha_{sd}\, R_{123}'$,
$T_{123}^{*} = T_{12}^{*}\, U_2^{*}$,
$U_2^{*} = (1 + S_2^{*})\,(1 - \alpha_{Rd2})$,
$S_2^{*} = R_{12}^{*}\, \alpha_{Rd2} / (1 - R_{12}^{*}\, \alpha_{Rd2})$,
$R_{12}^{*} = \alpha_{cd} + U_1^{*}\, \alpha_{Rd1}\,(1 - \alpha_{cd})$,
and
$R_{123}' = R_{12}' + \alpha_{Rd2} D_2 T_{12}^{*} + [S_2 + \alpha_{R2} t_c(\mu_o) t_{R1}(\mu_o)] t_{R1}(\mu) t_c(\mu)$.

Values for α_{sd} and ρ_s are estimated from the estimated clear-sky diffuse albedo α_{csd} (Minnis et al. 1993) and the observed clear-sky reflectance, ρ_{cs}.

$$\alpha_{sd} = 1.149\, \alpha_{csd} - 0.0333. \quad (3)$$

$$\rho_s = \rho_s' - D\, \alpha_{sd} / \exp(-\tau_{R13}/\mu_o), \quad (4)$$

where

$\rho_s' = [\rho_{cs} / \exp(-\tau_{gas}\,(1/\mu + 1/\mu_o)) - \rho_{R13}] / (1 - \alpha_{Rd13})$
$D = (1 + S)(1 - \alpha_{R13} - \exp(-\tau_{R13}/\mu_o) + S \exp(-\tau_{R13}/\mu_o)$,
$S = \alpha_{sd}\, \alpha_{Rd13} / (1 - \alpha_{sd}\, \alpha_{Rd13})$,
and
τ_{gas} is the absorption optical depth for the gaseous absorbers, such as ozone and water vapor, for the particular visible channel being used. This formulation does not explicitly account for any aerosols, so that the surface albedo and reflectance are actually more representative of the surface and aerosols combined.

The formulation of R_{as} was evaluated by comparing the AD results with (2) for the same set of surface, cloud, and viewing and illumination conditions. These conditions are comprised of a total of 12 surface albedos ranging from 4 to 90%, 12 cloud optical depths, from 0.5 to 128, 8 values of θ to 72.5°, 10 values of θ_o to 81.4°, and 15 values of ϕ. Two water droplet clouds with effective droplet radius r_e = 6 and 16 μm were used at cloud pressures p_c = 500 and 900 hPa. Two ice cloud models with effective ice crystal diameter D_e = 24 and 123 μm were used at p_c = 200 and 600 hPa. The differences $\Delta R\,(r, \tau, p_c, \alpha_{sd})$ between the results from the AD RTM and (2) were fit to a polynomial to minimize the differences:

$$\Delta R = a_o + \sum_{i=1}^{3} a_i \mu_o^{\,i} + \sum_{i=1}^{3} b_i \mu^{i} + \sum_{i=1}^{6} c_i \Theta^{i}, \quad (5)$$

where Θ is the scattering angle in radians. The reflectance at the top of the atmosphere for this model is

$$R_{TOA} = (R_{as} + \Delta R) \exp(-\tau_{gas}(1/\mu + 1/\mu_o). \quad (6)$$

The exponential term accounts for gaseous absorption and, in practice, varies with the altitude of the cloud.

When used for retrievals, the values of ΔR are computed for the specified values of α_{sd}, p_c, and r by linear interpolation and extrapolation between the values used to create the coefficients for (5). Equation (6) was tested for a wider range of various cloud models, surface albedos, and cloud pressures. The resulting relative differences between (6) and the AD calculations for those cases plus the original cases used in the formulation are summarized in Table 1 under the heading, "new parameterization." Results from the old parameterization from Minnis et al. (1993) are also shown to demonstrate the increase in accuracy and precision over the full range of surface albedo. The largest instantaneous errors occur for extreme values of θ, while the largest average errors for a given parameter occur for τ < 0.1. For example, the greatest average difference for a given ϕ in the low albedo range is 0.9% for τ = 0.5 at ϕ = 180°. Thus, if the AD TOA reflectance ρ_{TOA} is 6% ϕ = 180°, the average value from (6) is 6.06%. Overall, the differences are comparable to those between a high-resolution AD model and a discrete ordinates RTM (Y. Hu, personal communication 2001).

Because of its high accuracy for large surface albedos, (6) may be useful for simulating multilayered cloud reflectances in the following manner. The optical depth of the low-level cloud is first estimated in some independent manner such as the application of a microwave method (Lin et al. 1999) or by direct retrieval using nearby pixels without upper-level cloud contamination. The combination of the reflectances from the low-level cloud and the surface can be assumed to be a new surface and the terms α_{sd} and ρ_s are replaced in the parameterization by the new diffuse albedo and reflectance for the combined low-level cloud and surface layer.

This concept was tested by performing AD calculations for a range of conditions. The surface albedos are 0.04 and 0.20 with low-level clouds at p_c = 900 hPa, r_e = 10 μm, and τ = 2 - 64. The upper-level cloud is specified at p_c = 250 hPa, D_e = 68 μm, and τ = 0.25 - 8. A discrete set of angles was also specified: θ = 15, 45°; μ_o = 0.35, 0.75; and ϕ = 5, 35, 90, 135, and 175°.

Table 1. Relative differences in TOA reflectance between parameterization and AD calculations.

α_{sd} (%)	new parameterization	old parameterization
4-10	-0.01 ± 0.53 %	-0.08 ± 5.1 %
10 -50	-0.01 ± 0.67 %	-0.14 ± 7.0 %
50-90	0.03 ± 1.04 %	-4.3 ± 12.4 %

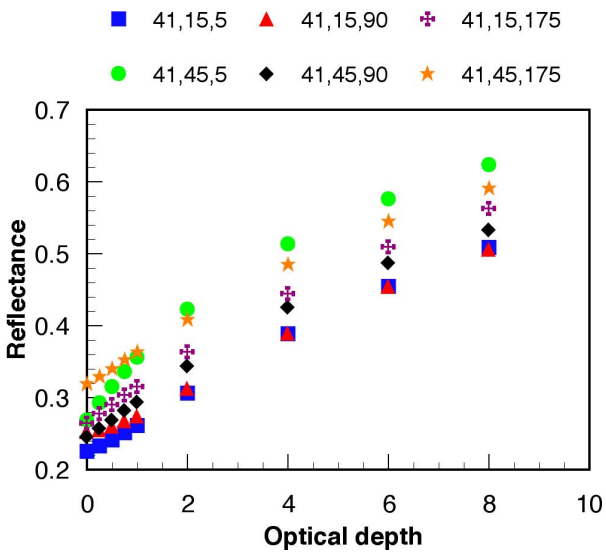

Fig. 1. TOA reflectance as function of τ_1 for D_e =68 μm from AD for τ_2 = 2 over a surface with albedo of 0.2. The numbers next to each symbol correspond to θ_o, θ, ϕ.

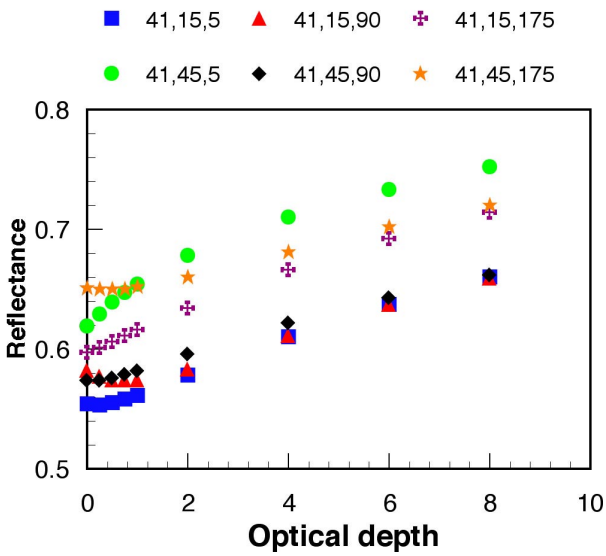

Fig. 2. Same as Fig. 1, except for τ_2 = 16.0 over surface with albedo of 0.2.

3. RESULTS

Figure 1 shows the variation of ρ_{TOA} with the upper cloud optical depth τ_1 over a low-level cloud with optical depth τ_2 = 2 over a surface with an albedo of 0.2 for θ_o = 41°. Each symbol corresponds to a different set of viewing angles. All of the reflectances increase monotonically with increasing τ_1. For a given value of τ_1, ρ_{TOA} is generally greater for the larger value of θ and smaller ϕ = 90°. The reflectances are usually greater for the backscattering direction except for the near sun-glint set of angles (41°, 45°, 5°). The relative variation of ρ_{TOA} for the given angle sets when τ_2 = 16 (Fig. 2) is similar to that in Fig. 1, except that the reflectance does not change monotonically with τ_1 in all cases. It is nearly constant for small values of τ_1 at certain viewing angles. For θ = 15° and ϕ = 90°, ρ_{TOA} actually decreases to a minimum at τ_1 = 1 before increasing. This darkening of a scene by a thin over thick cloud can often be observed from the window of a commercial aircraft.

Preliminary results for the parameterization are shown in Fig. 3 for the same conditions used for Fig. 1. In this case, the parameterization yields the same monotonic variation but under- and overestimates ρ_{TOA}, especially for larger values of τ_1. The behavior of R_{TOA} in Fig. 4 for the same conditions used in Fig. 2 is certainly different from that in Fig. 3 and is non-monotonic in one case. However, the parameterization captures little of the decrease in ρ_{TOA} for τ_1 < 2. At some of the angles, the drop in ρ_{TOA} is replaced by a significant increase in R_{TOA}. The model over- and underestimates the AD reflectances by up 0.02 in some cases. Fortunately, these results are some of the worst cases.

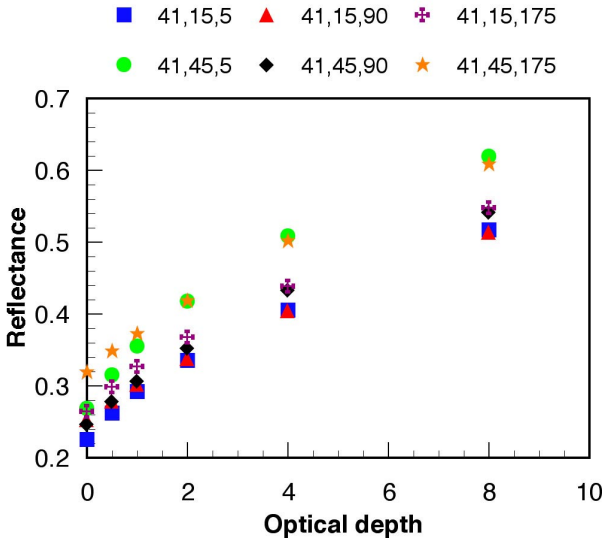

Fig. 3. Same as Fig. 1, except new parameterization is used instead of AD model.

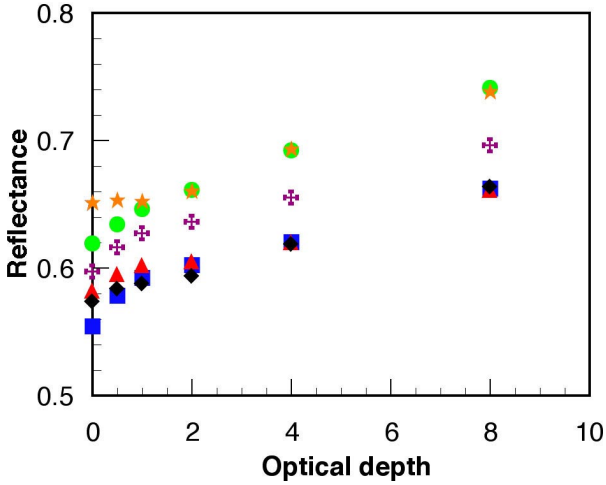

Fig. 4. Same as Fig. 2, except new parameterization is used instead of AD model.

Table 2. Mean relative differences in % between new parameterization and AD TOA reflectances for overlapped clouds as function of angle.

Angle	τ_2 = 0.5	1.0	2	4	8
θ_o = 41°	2.1	2.5	1.4	0.4	0.1
θ_o = 41°	-1.8	-2.3	-1.3	0.4	0.8
θ = 15°	2.9	3.5	2.7	1.6	0.8
θ = 45°	-2.1	-2.7	-2.2	-0.7	0.2
ϕ = 5°	-1.2	-1.1	-0.8	-0.3	-0.1
ϕ = 45°	-0.1	0.0	-0.1	0.0	0.1
ϕ = 90°	1.1	1.1	0.6	0.4	0.4
ϕ = 135°	0.9	0.7	0.7	1.1	1.0
ϕ = 175°	0.3	-0.1	0.0	0.9	0.9

A summary of the differences relative to the Ad results is given in Table 2 for α_s = 0.2. The average differences depend on the viewing and illumination angles as well as τ_1. The percent differences are smallest for larger values of τ_1, a result that is not surprising given that the multiple scattering for the thin cloud over a bright surface is more difficult to model. The mean differences are less than 1.1% when averaged over all solar and viewing zenith angles for a given relative azimuth angle. However, larger mean errors result for constant values of θ or θ_o. Overall, the mean difference and its standard deviation for all of the cases considered here for α_s = 0.2 is 0.001 $\pm$ 0.017, or 0.2% $\pm$ 3.0%. The differences are slightly larger for the lower-albedo surface: 0.002 $\pm$ 0.018 or 0.4% $\pm$ 3.2%.

The overall differences are substantially larger than those for the bright surfaces in Table 1. The latter were based on reflectance calculations that assumed that the underlying surface was a Lambertian reflector. The contributions of multiple scattering by the anisotropically reflecting lower cloud to the upwelling direct beam through the thin upper-level cloud may be different than the simple diffuse albedo term used in the formulation of (6). The new parameterization applied to multilayered clouds, however, produces more accurate results than those from the old parameterization for dark surfaces. However, for modeling multilayered clouds, an accuracy better than 3% would be desirable.

4. CONCLUDING REMARKS

Much additional research is required before drawing any firm conclusions about the utility of applying this approach to model reflectance fields from multilayered cloud systems. The results presented here can be considered as preliminary because alterations made in the code to utilize the cloud-surface calculations have not been thoroughly verified. Additionally, only a small set of angles and cirrus-stratus cloud combinations have been considered. A more thorough analysis using additional ice crystal effective diameters and a greater range of upper-level cloud optical depths will be used with other surface albedos and water droplet effective radii for the low-level cloud. Finally, the retrieval accuracy for upper level cloud optical depths will be examined by using this model to derive the optical depth from AD reflectance calculations.

Acknowledgments. This research was sponsored by the NASA Earth Science Enterprise Office through the CERES Project and by the Environmental sciences Division of the Department of Energy through the Atmospheric Radiation Measurement Program Interagency Agreement, DE-AI02-97ER62341.

REFERENCES

Baum. B. A. and J. D. Spinhirne, 2000: Remote sensing of cloud properties using MODIS airborne simulator imagery using SUCCESS, 3: cloud overlap. *J. Geophys. Res.*, **105**, 11793-11801.

Minnis, P., D. P. Garber, D. F. Young, R. F. Arduini, and Y. Takano, 1998: Parameterization of reflectance and effective emittance for satellite remote sensing of cloud properties. *J. Atmos. Sci.*, **55**, 3313-3339.

Minnis, P., Y. Takano, and K.-N. Liou, 1993: Inference of cirrus cloud properties using satellite-observed visible and infrared radiances, Part I: Parameterization of radiance fields. *J. Atmos. Sci.*, **50**, 1279-1304.

Lin, B., P. Minnis, B. A. Wielicki, D. R. Doelling, R. Palikonda, D. F. Young, and T. Uttal, 1998: Estimation of water cloud properties from satellite microwave and optical measurements in oceanic environments. II: Results. *J. Geophys. Res.*, **103**, 3887-3905.